Check for updates

Biomolecular conformational changes and ligand binding: from kinetics to thermodynamics†

Yong Wang, [iD] João Miguel Martins [iD] and Kresten Lindorff-Larsen [iD] *

The behaviour of biomolecular systems is governed by their thermodynamic and kinetic properties. It is thus important to be able to calculate, for example, both the affinity and rate of binding and dissociation of a protein–ligand complex, or the populations and exchange rates between distinct conformational states. Because these are typically rare events, calculating these properties from long molecular dynamics simulations remains extremely difficult. Instead, one often adopts a divide-and-conquer strategy in which equilibrium free-energy differences and the fastest state-to-state transition (*e.g.* ligand association or minor-to-major state conversion) are combined to estimate the slow rate (*e.g.* ligand dissociation) using a two-state assumption. Here we instead address these problems by using a previously developed method to calculate both the forward and backward rates directly from simulations. We then estimate the thermodynamics from the rates, and validate these values by independent means. We applied the approach to three systems of increasing complexity, including the association and dissociation of benzene to a fully buried cavity inside the L99A mutant variant of T4 lysozyme. In particular, we were able to determine both millisecond association and dissociation rates, and the affinity, of the protein–ligand system by directly observing dozens of rare events in atomic detail. Our approach both sheds light on the precision of methods for calculating kinetics and further provides a generally useful test for the internal consistency of kinetics and thermodynamics. We also expect our route to be useful for obtaining both the kinetics and thermodynamics at the same time in more challenging cases.

1 Introduction

Biomolecular processes are governed by their kinetic and thermodynamic properties, and the ability to determine these properties underlies both our fundamental understanding of biology, as well as our ability to optimize drug molecules or enzymes. Calculating protein–ligand binding thermodynamics, quantified in terms of binding free energies $\Delta G_{\text{binding}}$ or the equilibrium dissociation constant K_{d}, and kinetics characterized by association and dissociation constants (k_{on} and k_{off}), is a problem of critical importance in computational biology and computer-aided drug design.[1,2] When ligand binding can be described as a two-state system (Fig. 1), these quantities are related *via*

$$\Delta G_{\text{binding}} = k_{\text{B}} T \ln\left(\frac{K_{\text{d}}}{C^0}\right) = k_{\text{B}} T \ln\left(\frac{k_{\text{off}}}{k_{\text{on}} C^0}\right)$$

where k_{B} is the Boltzmann constant, T is the temperature and C^0 = 1 M is the standard reference concentration.

Structural Biology and NMR Laboratory, Linderstrøm-Lang Centre for Protein Science, Department of Biology, University of Copenhagen, Ole Maaløes Vej 5, DK-2200 Copenhagen N, Denmark. E-mail: lindorff@bio.ku.dk

† Electronic supplementary information (ESI) available. See DOI: 10.1039/c7sc01627a

Similarly to ligand binding, thermodynamics and kinetics are also linked in biomolecular conformational transitions, for example in protein folding. Indeed, one of the standard tests for whether protein folding conforms to a two-state model involves comparing the free energy difference estimated by equilibrium measurements with the value from kinetics.[3]

In principle, molecular dynamics (MD) simulations can provide a one-shot solution for calculating all of these properties. MD may, however, be limited by its inability to sample the long-timescale biological processes and the whole conformational space. Thus, although it has been possible to calculate rates (k_{folding} and $k_{\text{unfolding}}$) and thermodynamics ($\Delta G_{\text{folding}}$) from a single, long trajectory of protein folding,[4] this has only been possible at temperatures where $\Delta G \approx 0$. To our knowledge, the same problem has so far not been solved for ligand binding or for cases where the two rates differ substantially in magnitude.

Instead of pursuing a one-shot solution, one may take a divide-and-conquer strategy in which the thermodynamics and kinetics are calculated separately using different, but complementary techniques.[5–8] For the calculation of thermodynamics, several different methods have been developed. These methodologies can be categorized roughly into two types: enhanced sampling methods[9] and alchemical methods.[10,11] The enhanced sampling methods, including umbrella sampling (US),[12] non-equilibrium approaches[13] and metadynamics,[14] are
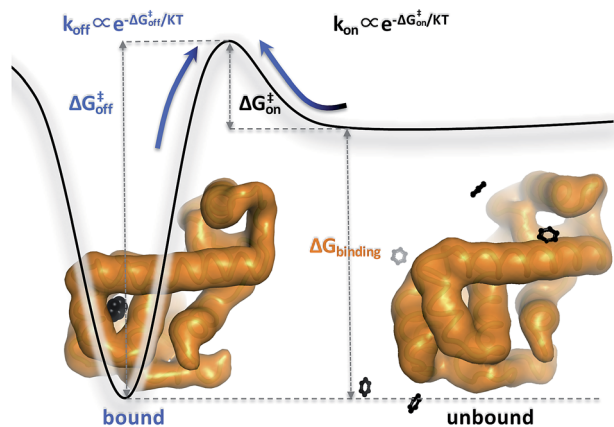
Fig. 1 A two-state model that demonstrates the relationship between kinetics and thermodynamics in protein–ligand binding. The free energy difference between the unbound and bound states is related to the binding affinity by $\Delta G_{binding} = k_{B}T \ln(K_{d}/C^{0})$. The free energy differences between the unbound and bound states with the transition state, $\Delta G_{on}^{\ddagger}$ and $\Delta G_{off}^{\ddagger}$, are related to the on and off rates, $k_{on} = A_{on} \, e^{-\Delta G_{on}^{\ddagger}/k_{B}T}$ and $k_{off} = A_{off} \, e^{-\Delta G_{off}^{\ddagger}/k_{B}T}$, respectively. The pre-exponential factors A_{on} and A_{off} are hard to measure and usually unknown. The complex of L99A mutant of T4L (orange) with benzene (black) serves as the model system to illustrate the bound and unbound states of protein–ligand systems.

based on the idea that an external bias is added to the original force field so as to make rare events occur more rapidly, but in a way that the unbiased free energy difference can be calculated by reweighting techniques.[15] The alchemical methods, including free-energy perturbation (FEP)[16] and thermodynamic integration,[17] are based on the idea that free energy differences can be calculated *via* a computationally convenient but not necessarily physical path because the free energy is a state function and path-independent.

While the free energy can often be calculated without knowing or studying the physical pathways that connect the reactant and product states (*e.g.* the bound and unbound states), the calculation of kinetics is generally more time-consuming and computationally expensive because the full physical reaction pathways have to be explored. It is still challenging but now possible to perform MD simulations up to a few milliseconds.[18] Focusing on ligand-binding, it has recently been demonstrated that it is possible to observe spontaneous binding of ligands to their targets, *e.g.* the cancer drug dasatinib to Src kinase,[19] the 'beta blocker' drugs propranolol and alprenolol to the β$_2$-adrenergic receptor,[6] a transition state analogue to the purine nucleoside phosphorylase enzyme[8] and benzamidine to the serine protease trypsin.[20–22] These observations demonstrate that the overall drug-binding process can successfully be observed starting from unbound states either in a few long trajectories[6,8,19,20] or multiple shorter trajectories (analysed *e.g.* with the help of Markov state models or the weighted ensemble path sampling).[21,23,24] The success of these examples results, in part, from the fact that the binding rate ($1/\tau_{on} = k_{on}[L]$) can be accelerated by simply increasing the ligand concentration [L]. However, to the best of our knowledge, unbiased MD simulations have yet not been used to determine the mechanism and kinetics of ligand escape for

a tight protein–drug complex. Although it is potentially possible to determine the off rates $\left(k_{off} = A_{off} \, e^{-\Delta G_{off}^{\ddagger}/k_{B}T} \right)$ from the height of the free energy barriers, $\Delta G_{off}^{\ddagger}$, this requires good reaction coordinates that represent the entire set of slowly varying degrees of freedom and also a good estimate of the pre-exponential factor A_{off} to convert barrier height to a rate. Finding good reaction coordinates and calculating the pre-exponential factor are other challenging tasks. Thus, k_{off} has usually been estimated from $\Delta G_{binding}$ and k_{on}, while assuming two-state kinetics.[6,8]

Inspired by the work of Grubmüller[25] and Voter,[26] Tiwary and Parrinello recently developed an enhanced sampling method, coined 'infrequent metadynamics',[9,27] to calculate the rate of a state-to-state transition. Metadynamics is an enhanced sampling method that discourages the system from sampling already visited conformational regions by continuously adding an external history-dependent repulsive potential at the present value of a small number of slowly changing order parameters, called collective variables (CVs).[14] The traditional objective of metadynamics simulations is to reconstruct the underlying free energy surface, or potential of mean force (PMF), as a function of the CVs used in the simulations or other order parameters. In standard metadynamics simulations it is very difficult to obtain kinetic properties.[28,29] The key idea of infrequent metadynamics is to bias the system with a frequency slow enough so that the transition state regions are not substantially biased; therefore the sequence of basin-to-basin transitions are unaffected and rates can be estimated by applying transition state theory. This method has recently been used to reproduce the kinetics of conformational change of a mutant of T4 lysozyme,[30] unbinding of the inhibitor benzamidine from trypsin,[31] the unfolding of the villin head-piece,[32] and state-to-state transitions of other model systems.[7,27,33]

Here we use MD simulations with the aid of infrequent metadynamics to address the relationship between thermodynamics and kinetics in three systems of increasing complexity. In systems of slow conformational transitions and ligand association/dissociation, we show that infrequent metadynamics provides the necessary accuracy and efficiency to determine the kinetic and thermodynamic properties. To distinguish the thermodynamic properties obtained from different sources, we term the free energies from enhanced sampling methods (*e.g.* metadynamics) or alchemical methods (*e.g.* FEP) as 'thermodynamic ΔG', while the free energies calculated from the forward and backward rates we call 'kinetic ΔG'. We in particular show that thermodynamic and kinetic ΔG values are generally consistent, even in cases where the rates are estimated from biased simulations or when the free energy landscape contains multiple intermediate states. In total, we provide a novel and feasible route to calculate kinetics and thermodynamics at the same time, and a useful consistency check for the calculated kinetic and thermodynamic parameters.

2 Results and discussion

In order to examine the accuracy and applicability of the proposed strategy, we applied it to three biomolecular systems

of increasing complexity. We first applied it to the conformational transition between α and β conformers of the alanine dipeptide (Ala2), a mostly two-state system. We then proceeded to study the conformational transitions between four metastable states of a five-residue peptide (Nme-Ala3-Ace). Finally, we applied the idea to the binding of a ligand to an internal, buried cavity in the L99A mutant of T4 lysozyme (L99A T4L). While the two peptide systems are sufficiently simple that the kinetics can be estimated from multiple, unbiased simulations, we demonstrate that infrequent metadynamics allows us also to determine kinetic and thermodynamic parameters for ligand binding to T4 lysozyme, further increasing the complexity of the test and the applicability of the method.

2.1 First example: two-state transitions in alanine dipeptide

The alanine dipeptide is perhaps the simplest 'biological molecule' and has been widely used as a model system for computational biologists since the first solvation simulation by Karplus *et al.* almost four decades ago.[34] Although this system has a simple topology, it shows a sufficiently complicated free energy landscape involving multiple conformational states (Fig. S1†). For simplicity, we projected the conformational space onto the slowest-relaxing degree of freedom, the dihedral angle Φ, to coarse-grain the system into two stable states, α and β (Fig. S2†). These two states are separated by high transition barriers, thus making the α ↔ β transition a typical rare event.

We estimated the free energy difference $\Delta G_{\alpha-\beta}^{PMF}$ between the two states to be 2.6 ± 0.1 kcal mol^{-1} by summing the populations on the both sides of the barrier. To calculate the kinetic $\Delta G_{\alpha-\beta}^{kine}$, we obtained the transition times, $\tau_{\alpha \to \beta}$ and $\tau_{\beta \to \alpha}$ for both directions (α to β and β to α) using the statistics from 40 independent unbiased MD simulations (Table 1). Due to the low computational cost to sample this model system, these simulations could be performed without enhanced-sampling techniques. From the calculated rates, we estimated $\Delta G_{\alpha-\beta}^{kine}$ to be $k_B T \ln(\tau_{\beta \to \alpha}/\tau_{\alpha \to \beta}) = 2.8 \pm 0.2$ kcal mol^{-1}, in excellent agreement with thermodynamic $\Delta G_{\alpha-\beta}^{kine}$ obtained from the potential of mean force.

2.2 Second example: four-state transitions in a five-residue peptide

We then proceeded to a more complex system, a five-residue peptide Ace-Ala3-Nme, whose energy landscape has multiple local minima, and where it is non-trivial how best to describe the free energy landscape by one or a few order parameters.[35,36] Using a recently described approach, called SGOOP (spectral gap optimization of order parameters), Tiwary *et al.* designed a one-dimensional reaction coordinate for this system

$(f = \sum_{i=1}^{6} a_i F(\theta)$, see Methods) as a linear function of six possible dihedral torsion angles.[36] We used this optimized CV in a standard metadynamics simulation (see Methods) which allowed us to obtain a converged free energy landscape (Fig. 2). The landscape reveals four free energy basins, separated by substantial barriers, indicating four conformational states that we labeled as A, B, C and D, respectively. The PMF allows us to estimate the free energy differences between states, ranging between 1.6 and 5.6 kcal mol^{-1} (Fig. 2).

Despite its simplicity, this model system displays a more complicated free energy landscape with multiple minima, and may thus serve as a relevant model for some of the complexities that one would expect to encounter in larger biological systems. In particular, this system violates the two-state assumption, allowing us to test the practical utility of our approach and the accuracy of free energy differences estimated from the kinetics in such cases. In particular, we asked the question: can we estimate all six free energy differences between states from the transition rates between states? If so, how precisely?

We obtained each transition time (*e.g.* $\tau_{A \to B}$) from 40 independent unbiased MD simulations starting from the corresponding reactant state (*e.g.* state A) and ending with the corresponding productive state (*e.g.* state B) (Table 2). In all cases but one, we observed complete state-to-state transitions for all 40 simulations. In the case of A-to-D transitions we observed only 28 successful events among 50 trials and 300 μs simulation time in total, and used a maximum likelihood method[37] to estimate of τ_{AD}.

The twelve transition times were subsequently used to estimate the six kinetic ΔG^{kine} values (Table 2). As in the case of the dipeptide, we find here also that the values are overall in very good agreement with ΔG^{PMF} estimated from the PMF (Fig. 3). The overall calculation of kinetic ΔG values achieved a mean
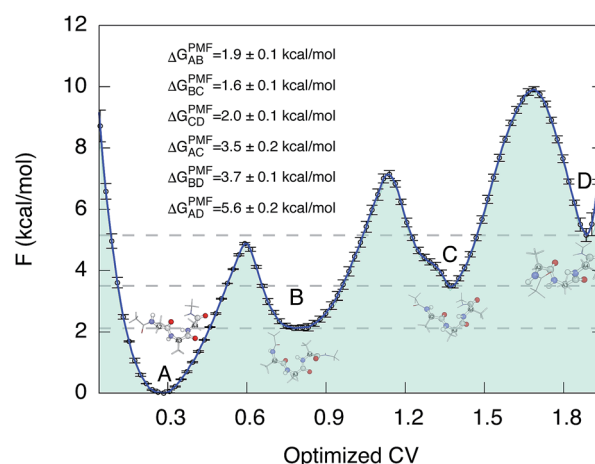
Fig. 2 Potential of mean force of Ace-Ala3-Nme at 300 K in implicit solvent. Representative conformations are shown next to the free energy basins. The potential of mean force as a function of the optimized collective variable allows us to estimate the free energy differences ΔG^{PMF} between these four basins. The convergence properties of free energy differences are shown in Fig. S3.†

Table 1 Transition times and kinetic and thermodynamic ΔG between α and β states of Ala2

$\tau_{\alpha \to \beta}$ (ns)	$\tau_{\beta \to \alpha}$ (ns)	$\Delta G_{\alpha-\beta}^{kine}$ (kcal mol^{-1})	$\Delta G_{\alpha-\beta}^{PMF}$ (kcal mol^{-1})
2.3 ± 0.6	231 ± 56	2.8 ± 0.2	2.6 ± 0.1

Table 2 Comparison between ΔG^{kine} and ΔG^{PMF} (in unit of kcal mol^{-1}) matrix of Ace-Ala3-Nme

$\tau_{A \to D}$	$\tau_{D \to A}$	$\Delta G_{AD}^{\text{kine}}$	$\Delta G_{AD}^{\text{PMF}}$
10.7 ± 2.0 μs	7.7 ± 1.0 ns	4.3 ± 0.2	5.6 ± 0.2
$\tau_{A \to C}$	$\tau_{C \to A}$	$\Delta G_{AC}^{\text{kine}}$	$\Delta G_{AC}^{\text{PMF}}$
722.4 ± 136.6 ns	6.9 ± 0.9 ns	2.8 ± 0.2	3.5 ± 0.2
$\tau_{A \to B}$	$\tau_{B \to A}$	$\Delta G_{AB}^{\text{kine}}$	$\Delta G_{AB}^{\text{PMF}}$
27.5 ± 5.1 ns	1.4 ± 0.5 ns	1.8 ± 0.3	1.9 ± 0.1
$\tau_{B \to C}$	$\tau_{C \to B}$	$\Delta G_{BC}^{\text{kine}}$	$\Delta G_{BC}^{\text{PMF}}$
23.3 ± 4.7 ns	3.0 ± 0.6 ns	1.2 ± 0.2	1.6 ± 0.1
$\tau_{B \to D}$	$\tau_{D \to B}$	$\Delta G_{BD}^{\text{kine}}$	$\Delta G_{BD}^{\text{PMF}}$
709.7 ± 130.0 ns	6.1 ± 1.6 ns	2.9 ± 0.2	3.7 ± 0.1
$\tau_{C \to D}$	$\tau_{D \to C}$	$\Delta G_{CD}^{\text{kine}}$	$\Delta G_{CD}^{\text{PMF}}$
8.1 ± 1.4 ns	0.5 ± 0.1 ns	1.7 ± 0.2	2.0 ± 0.1

absolute error (MAE) of 0.6 kcal mol^{-1} and a Pearson correlation coefficient of 0.99 with respect to ΔG^{PMF} from the converged free energy landscape.

We note that although we find a strong, linear correlation between ΔG^{PMF} and ΔG^{kine}, there appears to be a systematic deviation from a unity slope. This cannot easily be explained by lack of convergence of the free energy landscape (Fig. S3†) nor by how we estimate the rates (Table S1†). Instead we note that the deviations are only observed for the largest free energy

differences which also correspond to state-to-state transitions that cross one or two metastable states. In such cases, the processes will in general be multi-exponential and the dominant barrier might differ for the forward and backward reaction. Encouragingly, however, our results show that ΔG^{kine} still provides a rather accurate estimate of the free energy difference with an acceptable overall MAE, in the current case involving two metastable states. Overall, our results suggest that in practice it is possible to estimate the ΔG even when the free energy landscape and the intermediates are not fully known.

2.3 Infrequent metadynamics can get accurate kinetics but with less cost than unbiased MD

Because of the difficulty in unbiased MD simulations to sample slow transitions such as the A → D transition in the five-residue peptide described above, we further validated the calculation of $\tau_{A \to D}$, $\tau_{A \to C}$ and $\tau_{B \to D}$ by employing the recently developed 'infrequent metadynamics' approach.[9,27] We observed successful transitions in all simulations and estimated the corresponding unbiased transition times by reweighting the biased simulations (Table 3). The reliability of these estimates was analysed *a posteriori* by a Kolmogorov–Smirnov (KS) test,[38] in which the calculated *p*-value is used to test the null-hypothesis that the distribution of transition times is Poissonian. Here $p < 0.05$ would, for example, be indicative that the biased simulations after reweighting were non-Poissonian, and hence that the biasing had substantially perturbed the kinetics. In no case do we find low *p*-values, and the rates calculated from the infrequent metadynamics are generally very close to those obtained by unbiased simulations but obtained at 25–100 times less computational cost (Table 3).

2.4 Biological application: binding affinity estimation from association and dissociation times of a protein–ligand complex

The examples above, while simple, indicate that it is possible to determine thermodynamic properties from kinetics with reasonable accuracy even when intermediates are present, and
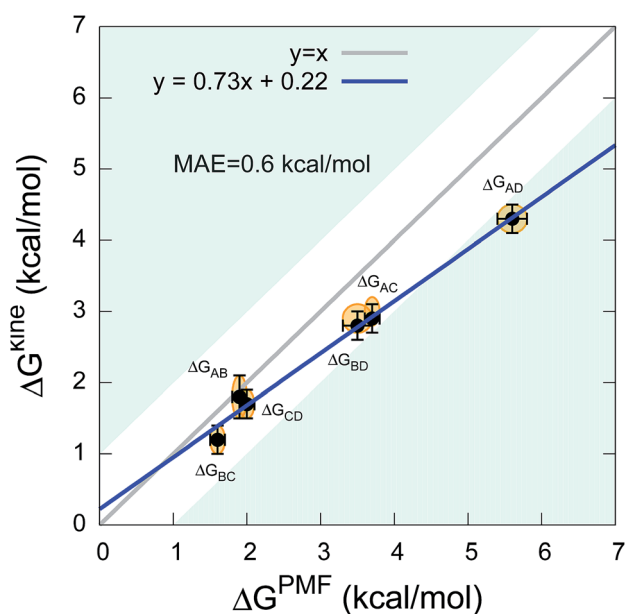

Fig. 3 Comparison between kinetic ΔG^{kine} and thermodynamic ΔG^{PMF} values in the state-to-state transitions of the five-residue peptide.

Table 3 Comparison of transition times of Ace-Ala3-Nme obtained from unbiased MD and infrequent metadynamics

	$\tau_{A \to D}$	*p*-Value	Cost
Unbiased MD	10.7 ± 2.0 μs		300 μs
InMetaD	16.4 ± 4.5 μs	0.41 ± 0.26	3 μs
	$\tau_{A \to C}$ (μs)	*p*-Value	Cost
Unbiased MD	722 ± 137 ns	0.34 ± 0.24	26 μs
InMetaD	553 ± 114 ns	0.50 ± 0.28	1 μs
	$\tau_{B \to D}$ (μs)	*p*-Value	Cost
Unbiased MD	709 ± 126 ns	0.48 ± 0.25	25 μs
InMetaD	765 ± 200 ns	0.34 ± 0.23	1 μs

that infrequent metadynamics simulations can also be used in cases where the kinetics is very slow. We thus finally proceed to illustrate the idea on a more biological and complex example of binding of a ligand to a protein. In particular, we study the L99A variant of T4 lysozyme (L99A T4L) in which the truncation of Leu99 to Ala creates a large internal cavity of volume $\sim 150 \text{ Å}^3$. It has been shown experimentally that this cavity can bind benzene and a variety of other aromatic ligands with sub-millimolar affinities, and with association times on the order of a millisecond (at mM concentration).[39–41] Since the binding site is fully buried inside the protein, ligand binding must be accompanied by conformational dynamics of the protein, and L99A T4L has thus become a model for understanding protein–ligand dynamics and interactions.[42–46]

Despite intensive research, several questions pertaining to the mechanism of ligand binding however remain open, in particular with the conformational dynamics underlying access to the internal site remaining unclear. Previous NMR experiments have shown that L99A T4L exchanges between a ground state and an alternative, higher-energy conformational state, but further structural studies showed that both of states are sterically inaccessible to incoming ligands.[41,45] This poses a long-standing question of how the ligands access the internal cavity buried in the protein core.[47–49] By using metadynamics simulations to explore the native state free energy landscape of L99A T4L in the absence of ligands, we recently discovered transiently formed tunnels that connect the interior binding site to the solvent,[30] and suggested these to be relevant for ligand binding.

Here we make a step forward by using enhanced sampling simulations to observe multiple events during which the ligand (benzene) either enters into or escapes from the buried cavity in L99A T4L. This not only provides us with valuable information on the ligand binding mechanism, but also allows us to determine ligand association and dissociation rates as well as binding thermodynamics. Here we focus on the kinetics and thermodynamics and analyse and describe the mechanistic aspects in future studies.

We used a total of $\sim$12 µs infrequent metadynamics simulations to collect 20 ligand association and 20 dissociation events. At the ligand concentration (5 mM) used in the simulation, we find τ_{on} and τ_{off} to be 9 ± 5 ms and 168 ± 59 ms, respectively (Fig. S4†). From these values we in turn determined on- and off-rates and compared these to experiments (Table 4). Also in this case, the KS test shows compatibility of the data with a Poisson process, though the relatively lower reliability for τ_{on} estimation suggests that binding events are more difficult to sample than the unbinding events.

From the calculated rates we also calculated the binding affinity, which we find to be in good agreement with the two experimental estimates from either calorimetric analysis[50] or NMR[39] (Table 4). To obtain an independent computational estimate of the binding affinity, we also performed an alchemical free energy calculation on the L99A T4L–benzene complex using the same force field. The result obtained ($\Delta G_{\text{binding}}^{\text{FEP}} = -4.9 \pm 0.1$ kcal mol^{-1}) is within error the same as that obtained from the ligand kinetics, demonstrating consistence between

Table 4 Comparison of simulation and experiment for binding of benzene to L99A T4L

	Simulation	Experiment
$k_{\text{on}}{}^a$	$3.5 \pm 2 \times 10^4 \text{ M}^{-1} \text{ s}^{-1}$	$8 \times 10^5 \text{ M}^{-1} \text{ s}^{-1}$
$k_{\text{off}}{}^b$	$7 \pm 2 \text{ s}^{-1}$	$800 \pm 200 \text{ s}^{-1}$
K_{d}	0.3 ± 0.1 mM	0.8 ± 0.12^c/ 0.2 ± 0.04^d mM
$\Delta G_{\text{binding}}$	-5.0 ± 0.6 kcal mol^{-1}	-4.2 ± 0.1^c/ -5.2 ± 0.2^d kcal mol^{-1}

^{a} p-Value of τ_{on} is 0.10 ± 0.12. ^{b} p-Value of τ_{off} is 0.38 ± 0.26. ^{c} Dissociation constant of 0.8 ± 0.12 mM is from ref. 39. ^{d} Dissociation constant of 0.2 ± 0.04 mM is from ref. 50.

these two completely different approaches. Finally, we note that even in a relatively long metadynamics simulation we were not able to obtain a converged equilibrium free energy landscape, and so could not estimate $\Delta G_{\text{binding}}^{\text{PMF}}$ in this case. The fact that we can estimate the free energy difference (from the kinetics) even in the case where equilibrium sampling is not possible, suggests that the approach could be useful in cases where other free energy methods are more difficult to apply such as when charged ligand alchemical modifications are needed or exact binding poses are not well known.

Although we obtained very good agreement between experiment and simulation for the ligand-binding thermodynamics, we note that both the on- and off-rates are one-to-two orders of magnitude too slow. Because of the internal consistency between the calculated rates and thermodynamics we suspect that the error is due to remaining force field discrepancies that manifest themselves in the rates more than in thermodynamics. Indeed, when parameterizing force fields one often focuses accuracy on the populated (free) energy minima.[51] Interestingly we also note a similar discrepancy between experimental rates of the conformational exchange of L99A T4L[30], and suggest that future research should focus on potential systematic biases in kinetic properties.

3 Discussion and conclusions

Here we have demonstrated the practical implementation of an approach that determines free energy differences for biomolecular rearrangements using the kinetics of the process. This is also possible using *e.g.* Markov state models, but the simpler approach taken here provides a convenient way to use enhanced sampling simulations to estimate the kinetics. We thus show that the approach is practically feasible and rather accurate, both in systems that violate the two-state assumption or that require further enhanced sampling to calculate the slow conformational rates. In the cases studied here, the free energy differences could be independently determined either by equilibrium sampling (peptide conformational dynamics) or free energy perturbation (ligand binding), and we find good agreement between the two approaches.

In other cases (such as conformational exchange in proteins[30]), it may be difficult to estimate the free energy

difference by these methods, and as we demonstrate here the calculation from kinetics is a viable alternative. Further, our finding of internal consistency between ligand affinity and rates in T4 lysozyme lends further support to the precision of the rates calculated by the enhanced sampling method used. This suggests also that these approaches can be used more generally to estimate the kinetics of ligand binding and escape. Further, we suggest that when calculating the kinetics of ligand binding and unbinding, it is useful to validate the results by comparing the kinetic free energy difference with that obtained *e.g.* from free energy perturbation.

4 Methods

4.1 Collective variables

Ala$_2$. We used the two dihedral angles Φ and Ψ in Ala2 as CVs in a 120 ns-long well-tempered metadynamics simulation to obtain the PMF, $F(\Phi)$. Gaussian hills were added every ps, with a starting height of 1.2 kJ mol^{-1}, width of 0.35, and bias factor of 10. The error bars of the potential of mean force were calculated from the difference between the free energy obtained by summing the deposited Gaussians and the one obtained with time-independent estimator.[15]

Ace-Ala$_3$-Nme. By using the method of spectral gap optimization of order parameters, Tiwary *et al.* designed a one-dimensional reaction coordinate for the five-residue peptide,

$$f = \frac{1}{2} \sum_{i=1}^{6} a_i \left(1 + \cos\left(\theta_i - \theta_i^{\text{Ref}} \right) \right)$$

as a linear function of six possibly relevant dihedral torsion angles.[36] Here θ_i^{Ref} is the reference dihedral angle. We used $\theta_i^{\text{Ref}} = 1.25$ and the coefficients are $a_i = \{0.6228, 0.1201, 0.5643, 0.1102, 0.5153, 0.0403\}$ as optimized previously[36] in three independent well-tempered metadynamics simulations (Fig. S3†). Gaussian hills were added every ps, with a starting height of 1.7 kJ mol^{-1}, width of 0.03 unit, and bias factor of 15.

L99A T4L–benzene. We recently used a non-equilibrium bias potential[52] to observe 20 trajectories of benzene escaping from the cavity of L99A T4L, and found a dominant unbinding pathway.[30] Here, we used contacts between the protein and ligand observed in these non-equilibrium paths to define a set of path CVs,[53] $S_{\text{path}}^{\text{Lig}}$ and $Z_{\text{path}}^{\text{Lig}}$ describing ligand association and dissociation. The two CVs quantify the progress along the path ($S_{\text{path}}^{\text{Lig}}$) and the distance away from the reference path ($Z_{\text{path}}^{\text{Lig}}$), respectively. Also, we previously demonstrated that a protein-centered CV ($S_{\text{path}}^{\text{Pro}}$) substantially enhances the native state dynamics of L99A T4L,[30] and so we used all three CVs in the simulations. Parameters and settings for the metadynamics simulations for Ace-Ala3-Nme and L99A T4L–benzene can be found in the ESI.†

4.2 Kinetics calculation

Briefly described, the infrequent metadynamics approach works by performing dozens (typically 10 to 40) individual simulations to obtain first passage times between the individual basins. These are then corrected by the known acceleration factors (decrease in barrier height due to the enhanced sampling) to obtain estimates of the unbiased rates. The acceleration factor can be calculated by appealing to generalized transition state theory:[54]

$$\alpha = \tau/\tau_{\text{M}} = \langle \text{e}^{V(s,t)/kT} \rangle_{\text{M}}$$

where the angular brackets denote an average over a metadynamics run before the first transition, and $V(s,t)$ is the metadynamics time dependent bias.

As the basin-to-basin transition is a rare event, its characteristic time is expected to be a Poisson-distributed random variable. In principle, its mean μ, standard deviation σ and median $t_{\text{m}}/\ln 2$ should be equal. In practice, however, they are somewhat sensitive to insufficient sampling, and so rather than simply calculating averages, we estimated the transition time τ from a fit of the empirical cumulative distribution function to the theoretical cumulative distribution function (TCDF):[38]

$$\text{TCDF} = 1 - \text{e}^{-\frac{t}{\tau}}$$

A bootstrap approach was used to estimate the errors. To examine whether the observed times indeed follow the expected Poisson distribution we used a KS test to obtain a p-value that quantifies the similarity between the empirical and theoretical distributions. The key parameters for infrequent metadynamics simulations, including the bias deposition pace and the initial bias height, are listed in Table 5.

In the unbiased simulations of Ace-Ala3-Nme we used a maximum likelihood method[37] to estimate of τ_{AD} because not all simulations reached the D state:

$$\tau_{\text{MLE}} = \frac{\sum_{i=1}^{n} t_i + \sum_{j=1}^{N-n} t_j}{n} \pm \frac{\sum_{i=1}^{n} t_i + \sum_{j=1}^{N-n} t_j}{n^{3/2}}$$

where t_i are the transition times for the n successful transition events and t_j are the lengths of the $N - n$ trajectories that have not transitions yet. In other cases where we could observe successful transition events in all trials either from unbiased MD simulations or infrequent metadynamics simulations, we calculated the transition times by fitting with TCDF as stated above.

4.3 Model systems and MD details

MD simulations were performed with GROMACS 5.1.2 (ref. 55) combined with the PLUMED 2.2 plugin for metadynamics.[56]

Table 5 Key parameters for obtaining kinetics from infrequent metadynamics

Simulation	$\tau_{\text{dep}}{}^a$ (ps)	h^b (kJ mol^{-1})
Transition of Ace-Ala3-Nme	200	0.4
Association of L99A T4L–BNZ	40	0.4
Dissociation of L99A T4L–BNZ	100	0.2

^{a} The deposition frequency of the Gaussian bias. ^{b} The height of the Gaussian bias.

For Ala2 and Ace-Ala3-Nme, the simulations were performed with Amber ff99SB force field[57] and an implicit solvent model.[58] The temperature was kept constant at 300 K using the v-rescale thermostat.[59] Bonds involving hydrogens were constrained using the LINCS algorithm. A time-step of 2 fs was used.

For L99A T4L–benzene system, the simulations were performed with the CHARMM22* force field[60] in the NPT ensemble using a periodic cubic box with a side length of 7 nm that includes ~10 000 water molecules. The temperature and pressure were kept constant at 298 K using the v-rescale thermostat[59] with a 1 ps coupling constant and at 1.0 bar using the Parrinello–Rahman barostat[61] with a 2 ps time coupling constant, respectively. We employed the virtual sites for hydrogen atoms with a single LINCS iteration (expansion order 6)[62] and constrained the bonds involving hydrogen atoms using the LINCS algorithm, allowing simulations to be performed with an integration time step of 4 fs. The long-range electrostatic interactions were calculated by the means of the particle mesh Ewald decomposition algorithm with a 0.16 nm mesh spacing.

4.4 $\Delta G_{binding}$ calculation by alchemical transformation

The DDM methodology[63] with the virtual bond algorithm[64] was used for the thermodynamic cycle calculation in GROMACS 5.0.6.[55] We ran three replicas for each λ value of the decoupling sequence and the results were combined using the Multistate Bennett Acceptance Ratio (MBAR).[65] The restraint atoms and potentials used were kept for all protein–ligand state calculations and replicas, in accordance with the DDM-VBA method, with increasing harmonic potential restrains starting from 0 and scaled to maximums of 4184 kJ mol^{-1} nm^{-2}, 41.84 kJ mol^{-1} rad^{-2} and 41.84 kJ mol^{-1} rad^{-2} for distance, angles and dihedrals respectively.

Acknowledgements

References

1 N. Ferruz and G. De Fabritiis, *Mol. Inf.*, 2016, **35**, 216–226.
2 M. De Vivo, M. Masetti, G. Bottegoni and A. Cavalli, *J. Med. Chem.*, 2016, **59**, 4035–4061.
3 S. E. Jackson and A. R. Fersht, *Biochemistry*, 1991, **30**, 10428–10435.
4 K. Lindorff-Larsen, S. Piana, R. O. Dror and D. E. Shaw, *Science*, 2011, **334**, 517–520.
5 R. O. Dror, D. H. Arlow, P. Maragakis, T. J. Mildorf, A. C. Pan, H. Xu, D. W. Borhani and D. E. Shaw, *Proc. Natl. Acad. Sci. U. S. A.*, 2011, **108**, 18684–18689.
6 R. O. Dror, A. C. Pan, D. H. Arlow, D. W. Borhani, P. Maragakis, Y. Shan, H. Xu and D. E. Shaw, *Proc. Natl. Acad. Sci. U. S. A.*, 2011, **108**, 13118–13123.
7 P. Tiwary, V. Limongelli, M. Salvalaglio and M. Parrinello, *Proc. Natl. Acad. Sci. U. S. A.*, 2015, **112**, E386–E391.
8 S. Decherchi, A. Berteotti, G. Bottegoni, W. Rocchia and A. Cavalli, *Nat. Commun.*, 2015, **6**, 6155.
9 O. Valsson, P. Tiwary and M. Parrinello, *Annu. Rev. Phys. Chem.*, 2016, **67**, 159–184.
10 J. D. Chodera, D. L. Mobley, M. R. Shirts, R. W. Dixon, K. Branson and V. S. Pande, *Curr. Opin. Struct. Biol.*, 2011, **21**, 150–160.
11 A. Perez, J. A. Morrone, C. Simmerling and K. A. Dill, *Curr. Opin. Struct. Biol.*, 2016, **36**, 25–31.
12 G. M. Torrie and J. P. Valleau, *J. Comput. Phys.*, 1977, **23**, 187–199.
13 C. Jarzynski, *Phys. Rev. Lett.*, 1997, **78**, 2690.
14 A. Laio and M. Parrinello, *Proc. Natl. Acad. Sci. U. S. A.*, 2002, **99**, 12562–12566.
15 P. Tiwary and M. Parrinello, *J. Phys. Chem. B*, 2014, **119**, 736–742.
16 R. W. Zwanzig, *J. Chem. Phys.*, 1954, **22**, 1420–1426.
17 J. G. Kirkwood, *J. Chem. Phys.*, 1935, **3**, 300–313.
18 R. O. Dror, R. M. Dirks, J. Grossman, H. Xu and D. E. Shaw, *Annu. Rev. Biophys.*, 2012, **41**, 429–452.
19 Y. Shan, E. T. Kim, M. P. Eastwood, R. O. Dror, M. A. Seeliger and D. E. Shaw, *J. Am. Chem. Soc.*, 2011, **133**, 9181–9183.
20 I. Buch, T. Giorgino and G. De Fabritiis, *Proc. Natl. Acad. Sci. U. S. A.*, 2011, **108**, 10184–10189.
21 N. Plattner and F. Noé, *Nat. Commun.*, 2015, **6**, 7653.
22 I. Teo, C. G. Mayne, K. Schulten and T. Lelièvre, *J. Chem. Theory Comput.*, 2016, **12**, 2983–2989.
23 D. Shukla, Y. Meng, B. Roux and V. S. Pande, *Nat. Commun.*, 2014, **5**, 3397.
24 M. C. Zwier, A. Pratt, J. L. Adelman, J. W. Kaus, D. M. Zuckerman and L. T. Chong, *J. Phys. Chem. Lett.*, 2016, **7**, 3440–3445.
25 H. Grubmüller, *Phys. Rev. E: Stat. Phys., Plasmas, Fluids, Relat. Interdisc. Top.*, 1995, **52**, 2893.
26 A. F. Voter, *J. Chem. Phys.*, 1997, **106**, 4665–4677.
27 P. Tiwary and M. Parrinello, *Phys. Rev. Lett.*, 2013, **111**, 230602.
28 F. Pietrucci, F. Marinelli, P. Carloni and A. Laio, *J. Am. Chem. Soc.*, 2009, **131**, 11811–11818.
29 F. Marinelli, F. Pietrucci, A. Laio and S. Piana, *PLoS Comput. Biol.*, 2009, **5**, e1000452.
30 Y. Wang, E. Papaleo and K. Lindorff-Larsen, *eLife*, 2016, **5**, e17505.
31 P. Tiwary, J. Mondal, J. A. Morrone and B. Berne, *Proc. Natl. Acad. Sci. U. S. A.*, 2015, **112**, 12015–12019.
32 H.-J. Tung and J. Pfaendtner, *Mol. Syst. Des. Eng.*, 2016, **1**, 382–390.
33 D. Callegari, A. Lodola, D. Pala, S. Rivara, M. Mor, A. Rizzi and A. M. Capelli, *J. Chem. Inf. Model.*, 2017, **57**, 159–169.
34 P. J. Rossky and M. Karplus, *J. Am. Chem. Soc.*, 1979, **101**, 1913–1937.
35 O. Valsson and M. Parrinello, *J. Chem. Theory Comput.*, 2015, **11**, 1996–2002.
36 P. Tiwary and B. Berne, *Proc. Natl. Acad. Sci. U. S. A.*, 2016, 201600917.

37 B. Zagrovic and V. Pande, *J. Comput. Chem.*, 2003, **24**, 1432–1436.

38 M. Salvalaglio, P. Tiwary and M. Parrinello, *J. Chem. Theory Comput.*, 2014, **10**, 1420–1425.

39 V. A. Feher, E. P. Baldwin and F. W. Dahlquist, *Nat. Struct. Biol.*, 1996, **3**, 516–521.

40 F. A. Mulder, A. Mittermaier, B. Hon, F. W. Dahlquist and L. E. Kay, *Nat. Struct. Mol. Biol.*, 2001, **8**, 932–935.

41 G. Bouvignies, P. Vallurupalli, D. F. Hansen, B. E. Correia, O. Lange, A. Bah, R. M. Vernon, F. W. Dahlquist, D. Baker and L. E. Kay, *Nature*, 2011, **477**, 111–114.

42 W. A. Baase, L. Liu, D. E. Tronrud and B. W. Matthews, *Protein Sci.*, 2010, **19**, 631–641.

43 S. E. Boyce, D. L. Mobley, G. J. Rocklin, A. P. Graves, K. A. Dill and B. K. Shoichet, *J. Mol. Biol.*, 2009, **394**, 747–763.

44 K. Wang, J. D. Chodera, Y. Yang and M. R. Shirts, *J. Comput.-Aided Mol. Des.*, 2013, **27**, 989–1007.

45 P. Vallurupalli, N. Chakrabarti, R. Pomes and L. Kay, *Chem. Sci.*, 2016, **7**, 3602–3613.

46 R. Kitahara, Y. Yoshimura, M. Xue, T. Kameda and F. A. Mulder, *Sci. Rep.*, 2016, **6**, 20534.

47 F. A. Mulder, B. Hon, D. R. Muhandiram, F. W. Dahlquist and L. E. Kay, *Biochemistry*, 2000, **39**, 12614–12622.

48 C. J. López, Z. Yang, C. Altenbach and W. L. Hubbell, *Proc. Natl. Acad. Sci. U. S. A.*, 2013, **110**, E4306–E4315.

49 M. Merski, M. Fischer, T. E. Balius, O. Eidam and B. K. Shoichet, *Proc. Natl. Acad. Sci. U. S. A.*, 2015, **112**, 5039–5044.

50 A. Morton, W. A. Baase and B. W. Matthews, *Biochemistry*, 1995, **34**, 8564–8575.

51 K. Lindorff-Larsen, S. Piana, K. Palmo, P. Maragakis, J. L. Klepeis, R. O. Dror and D. E. Shaw, *Proteins: Struct., Funct., Bioinf.*, 2010, **78**, 1950–1958.

52 M. Marchi and P. Ballone, *J. Chem. Phys.*, 1999, **110**, 3697–3702.

53 D. Branduardi, F. L. Gervasio and M. Parrinello, *J. Chem. Phys.*, 2007, **126**, 054103.

54 P. Hänggi, P. Talkner and M. Borkovec, *Rev. Mod. Phys.*, 1990, **62**, 251.

55 M. J. Abraham, T. Murtola, R. Schulz, S. Páll, J. C. Smith, B. Hess and E. Lindahl, *SoftwareX*, 2015, **1**, 19–25.

56 G. A. Tribello, M. Bonomi, D. Branduardi, C. Camilloni and G. Bussi, *Comput. Phys. Commun.*, 2014, **185**, 604–613.

57 V. Hornak, R. Abel, A. Okur, B. Strockbine, A. Roitberg and C. Simmerling, *Proteins: Struct., Funct., Bioinf.*, 2006, **65**, 712–725.

58 A. Onufriev, D. Bashford and D. A. Case, *Proteins: Struct., Funct., Bioinf.*, 2004, **55**, 383–394.

59 G. Bussi, D. Donadio and M. Parrinello, *J. Chem. Phys.*, 2007, **126**, 014101.

60 S. Piana, K. Lindorff-Larsen and D. E. Shaw, *Biophys. J.*, 2011, **100**, L47–L49.

61 M. Parrinello and A. Rahman, *J. Appl. Phys.*, 1981, **52**, 7182–7190.

62 K. A. Feenstra, B. Hess and H. J. Berendsen, *J. Comput. Chem.*, 1999, **20**, 786–798.

63 M. K. Gilson, J. A. Given, B. L. Bush and J. A. McCammon, *Biophys. J.*, 1997, **72**, 1047–1069.

64 S. Boresch, F. Tettinger, M. Leitgeb and M. Karplus, *J. Phys. Chem. B*, 2003, **107**, 9535–9551.

65 M. R. Shirts and J. D. Chodera, *J. Chem. Phys.*, 2008, **129**, 124105.